Materials Futures

Dongguan Institute of Materials Science and Technology, CAS

Scale-up synthesis of perovskite nanocrystal/cellulose chiral ink toward patterned and circularly polarized luminescence

To cite this article: Boya Li *et al* 2026 *Mater. Futures* **5** 025301

OPEN ACCESS
IOP Publishing | Dongguan Institute of Materials Science and Technology, CAS
MATERIALS FUTURES
Mater. Futures 5 (2026) 025301 (11pp)
https://doi.org/10.1088/2752-5724/ae3592

Scale-up synthesis of perovskite nanocrystal/cellulose chiral ink toward patterned and circularly polarized luminescence

Boya Li[1,3], Leimeng Xu[2,3,*], Wenxuan Fan[2], Fangru Wang[1], Wanjie Wang[1,*] and Jizhong Song[2,*]

[1] School of Materials Science and Engineering, Zhengzhou University, Daxue Road 75, Zhengzhou 450052, People's Republic of China
[2] Key Laboratory of Materials Physics of Ministry of Education, Laboratory of Zhongyuan Light, School of Physics, Zhengzhou University, Zhengzhou 450051, People's Republic of China

E-mail: xuleimeng@zzu.edu.cn, wwj@zzu.edu.cn and songjizhong@zzu.edu.cn

Received 8 September 2025, revised 22 December 2025
Accepted for publication 8 January 2026
Published 2 February 2026

Abstract

Circularly polarized luminescence perovskite nanocrystals (NCs) hold great potential in the field of information encryption, 3D display and spintronics. However, the synthesis of the chiral perovskites is still confronted with various problems, such as cumbersome synthesis process, poor compatibility and limited processability, which impede their further implementation. In this study, a one-step wet-ball-milling method is proposed for the scale-up synthesis (up to 500 mL) of chiral perovskite ink, where the chiral molecule R-/S-1,2-diphenylethylenediamine (R-/S-DPEM) are introduced as chiral initiator. Chiral R-/S-DPEM molecules can endow the chirality to perovskite NCs through the strong coupling with perovskite surface. Specifically, ethyl cellulose is incorporated as passivating agents and structural supporting molecules, which can not only passivate the perovskite NCs and improve their stability, but also enable the chiral ink to possess better processability. The obtained ink is compatible with multiple substrates, which can be directly processed into various luminescent patterns by means of screen printing, writing, impregnation, laser engraving, etc. These patterns demonstrate high storage stability, flexibility and water resistance, fulfilling the requirements of a wide range of occasions in the future. This work provides a feasible solution for scalable synthesis of chiral perovskite inks, which offer promising prospects in optical anti-counterfeiting, information encryption and wearable optoelectronic devices.

[3] These authors contributed equally.
[*] Authors to whom any correspondence should be addressed.

Supplementary material for this article is available online

Keywords: perovskite, CPL, ethyl cellulose, scale-up synthesis, chiral ink

1. Introduction

Circularly polarized luminescence (CPL) has attracted enormous attention in the fields of 3D display [1, 2], information encryption [3, 4] and spintronics [5, 6], due to its advantages in light field adjustability, chiral optical activity uniqueness, and spin-polarization coupling effect [7]. Among various chiral nanomaterials, metal halide perovskite possesses remarkable properties, such as tunable emission wavelength, high photoluminescence (PL) efficiency, and solution processability [8–11], which is considered one of the most effective luminescent carriers for encoding chiral information [12, 13]. In general, to endow perovskite with excellent luminescent properties, it is crucial to achieve high exciton binding energy by reducing the dimension to nanoscale. Thus, the chiral properties of perovskite nanocrystals (NCs) have garnered enormous attention [14–16]. In 2020, Kim *et al* [17]. Modified $FAPbBr_3$ NCs with chiral ligand (R)-2-octylamine to achieve CPL with dissymmetry factor (g_{lum}) = 6.8×10^{-2}. Mendoza-Carreño *et al* [18]. Fabricated a two-dimensional chiral superstructure using nano-imprinting technology and coated the surface with perovskite NCs, achieving a g_{lum} value of 0.16. These reports demonstrate the significance of chiral-active perovskite NCs in advancing fundamental research and future practical application.

Currently, the acquisition of chiral perovskite NCs is primarily achieved through the following approaches: i) passivating perovskite NCs with chiral ligands [17, 19, 20], ii) inserting chiral A-site cations into perovskites [21–23], and iii) introducing perovskite NCs to the chiral structure environment (e.g. resonant interaction of chiral metasurface and cholesteric liquid crystal) [24–27]. Compared with the latter two strategies, engendering chirality to perovskite NCs via chiral ligands exhibits better operability and better PL properties. However, the large-scale synthesis of chiral perovskites is still hindered by the complex preparation process, e.g. hot injection or recrystallization method, which involves multiple steps and a cumbersome purification process, not conducive to scalable production [28]. Therefore, exploring concise synthesis strategy is of vital importance for the large-scale production of chiral perovskite NCs.

Furthermore, the application scenarios of the chiral perovskite NCs are also limited by poor stability and weak processability. In order to obtain processable and stable chiral luminescent perovskite NCs inks, introducing polymers are feasible strategies by embedding chiral perovskite NCs into polymer matrix. For example, Kim *et al* [29]. Proposed a strategy based on block copolymer micelles for chiral perovskites, which could effectively protect perovskite NCs from moisture, heat and air. Wen *et al* [30]. Reported chiral perovskite nanosheet/PAN/PS double matrix core-shell nanofibers, which significantly enhanced storage stability of perovskite. These studies indicate that incorporation of polymers can effectively enhance the stability perovskite NCs. Compared with petroleum-based polymers, bio-based polymer, cellulose materials, not only possess high processability, but also have the advantages of low cost, renewability, degradability and abundant resources, becoming promisingly popular in the field of optoelectronics. For example, Wang *et al* [31]. Utilized an ionized cellulose derivative, C–Im–CN, to effectively promote the oriented growth of perovskite crystals and control defects, achieving a photoelectric conversion efficiency of 24.71% along with excellent long-term stability. Song *et al* [32]. Incorporated $CsPb(Br_{0.4}I_{0.6})_3$ into ethyl cellulose (EC) solution, due to the passivation property of EC, the perovskite film encapsulated by EC maintains better stability in water compared to PMMA film. The integration of cellulose-based polymers has opened up new possibilities for the development of perovskite chiral materials.

In this work, we propose a simple, one-step wet-ball-milling strategy for the scale-up synthesis of chiral perovskite NCs/EC ink for the patterned CPL. Herein, a highly asymmetric chiral molecule, R- or S-1,2-diphenylethylenediamine (R-/S-DPEM) is introduced as chiral initiator. EC not only improves the processability of the CPL ink for various patterned CPL films, but also passivates perovskite NCs surfaces through hydroxyl and ethoxy groups, thereby enhancing luminescence efficiency and stability. Ultimately, high-efficiency CPL perovskite inks with a g_{lum} of up to 2.7×10^{-3} (R-$CsPbBr_3$/EC) and -3.4×10^{-3} (S-$CsPbBr_3$/EC) are achieved. Furthermore, CPL inks with tunable colors are successfully obtained via anion exchange. Benefiting from the processability of EC, this ink can be directly used for writing and screen printing, processed into fluorescent patterns, and exhibits compatibility with diverse substrates. Large-area circularly polarized luminescent films are also fabricated and exhibit excellent flexibility and stability. This highly processable CPL ink exhibits significant application potential in future optoelectronic devices.

2. Method

2.1. Materials

CsBr (99.9%), FABr (99.9%), Oleylammonium Chloride (OAmCl, 99.5%), Oleylammonium Iodide (OAmI, 98%) were purchased from Xi'an Polymer Light Technology Corp. $PbBr_2$ (99.9%), (EC, 80–120 mPa.s, ethoxy: 48.5%–49.5%), octylamine (99%) were acquired from Macklin Inc. (1 R,2 R)-(+)-1,2-Diphenylethylenediamine (R-DPEM, 99%), (1 S,2 S)-(-)-1,2-Diphenylethylenediamine (S-DPEM, 99%) were purchased from InnoChem Science & Technology Co., Ltd Toluene (AR) was obtained from LuoYang Chemical

Reagent Factory. All reagents were employed as received without further purification.

2.2. Preparation of $CsPbBr_3$/EC ink

$CsPbBr_3$/EC ink was prepared by ball-milling method. First, 60 μL of octylamine and 15 mL of toluene were mixed evenly and put into an agate grinding jar. Then, 0.15 mmol (0.0188 g) of FABr, 0.85 mmol (0.181 g) of CsBr, 1 mmol (0.367 g) of $PbBr_2$ and 0.5 g of EC were transferred to the agate grinding jar and stirred at the speed of 600 rpm for 4 h at room temperature without the protection of inert gas. Subsequently, 0.2 mmol, 0.4 mmol and 0.6 mmol of R-/S-DPEM were added to the jar respectively and continued grinding for 1 h.

2.3. Preparation of $CsPbX_3$/EC ink

We used anion exchange method to prepare blue and red fluorescent inks. Similarly, after $CsPbBr_3$/EC was stirred for 4 h, OAmCl or OAmI were added for 1 h ball milling. Subsequently, R-/S-DPEM were added to the jar respectively and continued grinding for 1 h.

2.4. Characterization

Steady-state PL measurements were performed at room temperature in an atmospheric environment. All $CsPbBr_3$/EC film samples were excited at 365 nm, and the spectra were collected on a Hitachi F-4700 spectrofluorometer equipped with a Xenon arc lamp. The instrument settings included an emission range of 400–700 nm, a scan speed of 1200 nm min^{-1}, EX/EM slit widths of 5.0 nm, and a PMT voltage of 250 V. The Olympus DSX1000 microscope was used to record the fluorescence images. All CPL spectra were measured at room temperature on a JASCO CPL-300 spectrometer. PL mapping was carried out on Fluorescent-Raman optical system (Zolix) under excitation by a 420 nm laser. Time-resolved PL (TRPL) of the $CsPbBr_3$/EC composites was performed by the Spectrometer (Edinburgh FLS-980, UK). Crystal structure was collected on an x-ray diffractometer (SmartLab-SE, Japan). Fourier transform infrared (FTIR) spectra were tested on Nicolet iS 5 (Thermo Scientific). X-ray photoelectron spectroscopy (XPS) (ESCALAB 250Xi, Thermo Fisher Scientific) was used to analyze the valence state. Scanning electron microscope (Zeiss Gemini 300, Germany) and High-resolution transmission electron microscope (JEOL 2100 F, 200 KV) were used to observe the appearance. Elemental mapping analysis was carried out by energy-dispersive x-ray spectroscopy (EDS) using an INCA X-Act instrument.

3. Results and discussion

The $CsPbBr_3$/cellulose ink was prepared by a wet-ball-milling method, the diagram of the synthesis process is shown in figure 1(a). Typically, the long chain polymer EC, Cs and Pb salts, chiral molecules (R- or S-1, 2-diphenylethylenediamine (R-/S-DPEM)), auxiliary ligands and toluene were transferred into the ball mill jar, after high-speed rotation for several hours, the chiral ligand-perovskite NCs were grown *in situ* in the EC cross-linked network. Surface-enriched chiral molecules impart chiral characteristics to perovskite NCs, while highly cross-linked EC molecules provide additional structural stability and functionality. The entire process is conducted under ambient conditions, demonstrating the simplicity and practicability of our method. This method exhibits the advantage in enabling the scalable production of high-quality chiral perovskite NCs inks, which is evidenced by the photograph of 500 mL chiral perovskite NCs ink in figure 1(b). The obtained ink could be directly processed into paper-based films via scrap coating (figure 1(c)). Compared to traditional method (e.g. hot injection), the proposed wet ball-milling method reveals more advantages, such as higher yield (scalability), better simplicity (without inert gases, complex solvent system or high temperatures). Benefiting from EC, chiral perovskite exhibits excellent stability (passivation and protection), processability (patterned and film formation) than bare perovskite NCs. Furthermore, EC, as a biomass material, offers the key advantage of renewability, which petroleum-based polymers lack. This work achieves an effective trade-off between scalable synthesis and direct application (figure 1(d)).

The crystal structure of the $CsPbBr_3$/EC composite was investigated by x-ray diffraction (figure S1), the series of lattice diffraction peaks marked in the figure correspond to $CsPbBr_3$ (PDF#54-0752). At the same time, there are also a few diffraction peaks of Cs_4PbBr_6, corresponding to PDF#73-2478. The microtopography of $CsPbBr_3$/EC presented in figures 2(a) and (b) shows that the perovskite NCs distribute across the EC matrix, offering enhanced growth space for perovskite NCs, thereby facilitating their structural optimization and stability. High-resolution TEM (HRTEM) reveals the clear lattice spacing of 0.29 nm, which is in good agreement with the (200) plane of the cubic $CsPbBr_3$. The slightly decreased average particle size of $CsPbBr_3$/EC (figure S2) is attributed to the confining effect of the EC molecular chains on the growth of NCs, as well as the strong interaction between the functional groups of EC and $CsPbBr_3$ NCs. The components of $CsPbBr_3$/EC are further analyzed via selective EDS elemental mapping, as shown in figures 2(c)–(i). Cs, Pb, Br, are uniformly distributed throughout the selected perovskite NCs, while C, O, N originate from cellulose molecules and surface ligands on perovskite NCs surface.

In this system, EC molecules, composed of repeating six-membered heterocyclic units functionalized with hydroxyl and ethyl ether groups, can form interwoven networks through sharing O to form flexible paper substrates (figure 3(a)). Moreover, O in the ether may coordinate with uncoordinated Pb^{2+}, while H in the hydroxyl group forms dipole interaction with the Br^- in perovskite NCs [33, 34]. Chiral molecules, R-/S-DPEM, are enriched on the surface of perovskite NCs via interaction between amine groups and halogens, transfer the asymmetric structure to perovskite NCs [35–37]. The effective cross-linking of EC molecules not only can protect the perovskite nanoparticles and enhance the stability of the ink, but also facilitate the subsequent processing and treatment.

FTIR spectroscopy was conducted to verify the chemical interaction between EC and the perovskite NCs. As shown in

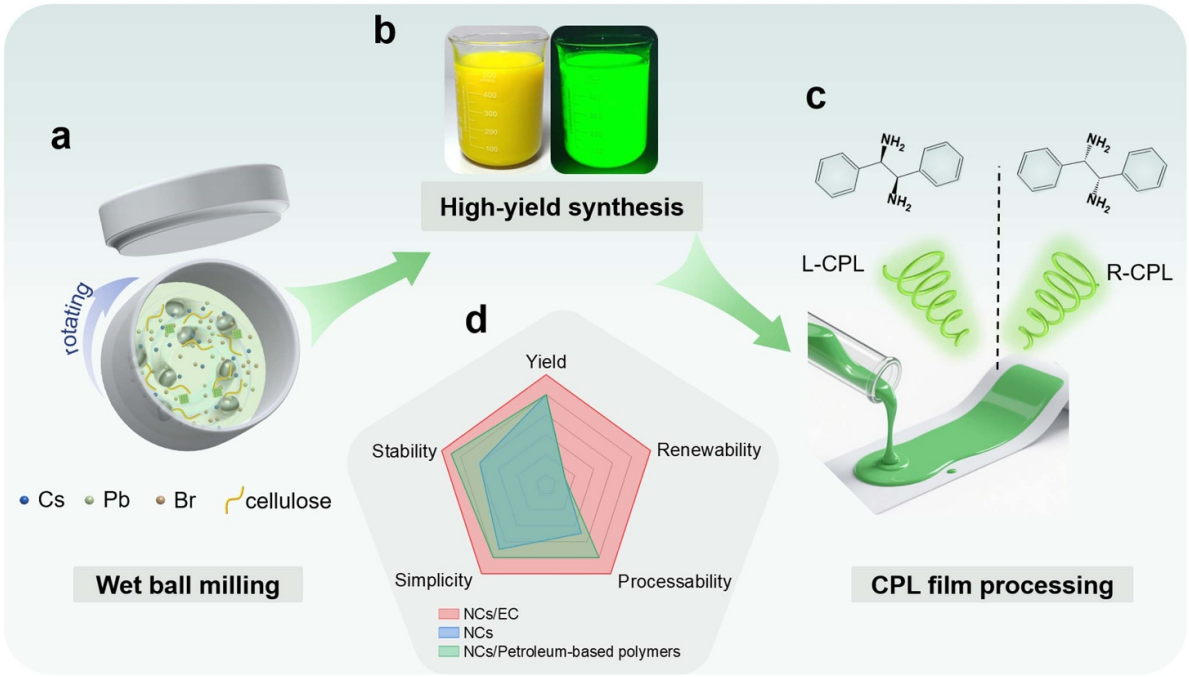

Figure 1. Schematic diagram of synthesis. (a) Schematic illustration of synthesizing $CsPbBr_3$/EC ink by wet-ball-milling. (b) Photographs of 500 mL $CsPbBr_3$/EC ink under natural light and UV light. (c) Schematic illustration of fabricating chiral $CsPbBr_3$/EC film with CPL. (d) Radar charts compare the features of different systems for perovskite NCs.

figure 3(b), the vibration peaks of C–O–C bond at 1110 cm^{-1} and –OH bond at 3484 cm^{-1} originated from EC molecule, which is absent in control $CsPbBr_3$. Meanwhile, the vibration peak of C–O–C in $CsPbBr_3$/EC shifts from 1110 to 1055 cm^{-1} and –OH shifts from 3484 to 3509 cm^{-1}, which demonstrates the interaction between EC and the perovskite NCs. Furthermore, we also employed XPS to investigate the interaction between the perovskite NCs and EC. The O 1s binding energy serves as a probe for the interaction mechanism, given the abundance of oxygen atoms from the ether groups in the EC molecule. The O 1s signal at 531.1 eV, characteristic of C–O–C bonds, is observed only in the $CsPbBr_3$/EC ink and serves as direct proof of EC's presence (figure 3(c)). As shown in figure 3(d), the binding energy of Pb 4f state of $CsPbBr_3$/EC shifts to higher energy compared to $CsPbBr_3$ (138.0 eV to 138.3 eV for $4f_{7/2}$ and 142.9 eV to 143.2 eV for $4f_{5/2}$, respectively). In addition, compared with $CsPbBr_3$, the binding energies of Br $3d_{5/2}$ and Br $3d_{3/2}$ of $CsPbBr_3$/EC shift from 68.0 eV to 67.8 eV and from 69.0 eV to 68.8 eV, respectively, indicating the formation of strong hydrogen bonding interactions between –OH in cellulose and Br^- (figure 3(e)). The observed binding energy shifts for Pb 4f and Br 3d reveal an interaction between EC and the Pb^{2+} and Br^- ions of the octahedron. From the above analysis, it is evident that cellulose molecules can effectively passivate the surface of perovskite NCs through interaction.

Benefiting from the effective passivation of EC, the PL performance of $CsPbBr_3$/EC ink is greatly improved. The PL spectra of the synthesized $CsPbBr_3$ and $CsPbBr_3$/EC inks and the photographs under UV light are shown in figure 3(f). The TRPL shows that $CsPbBr_3$/EC ink reveals a longer average lifetime of 32.3 ns compared to that of $CsPbBr_3$ (18.6 ns) as shown in figure 3(g). Meanwhile, the PLQY test showed an increase from 56% of $CsPbBr_3$ to 83% of $CsPbBr_3$/EC (figure S3). In addition, the $CsPbBr_3$/EC ink retains 80% of its initial brightness after being stored in the surrounding environment for 100 d, which is superior to the 50% of $CsPbBr_3$, demonstrating greatly enhanced stability. The intensity variation curve and the pictures under natural light are shown in figure 3(h). These findings indicate that EC can effectively passivate defects and improve radiative recombination of perovskite NCs.

On the basis of the aforementioned high-quality luminescent $CsPbBr_3$/EC ink, the incorporation of chiral ligand R-/S-DPEM enhances the luminescent properties of the inks. As shown in figures S4(a) and (b), the PL intensity shows a trend of increasing first and then decreasing with the increase of the concentration of chiral ligands, and it reaches the optimal value at 0.6 mmol, and a slight blue shift occurs. The absorption peaks of the UV-Vis spectra (figures S4(c) and (d)) show no other obvious absorption peaks. Furthermore, the introduction of chiral surface ligands R-/S-DPEM leads to the coupling of electronic states between perovskite NCs. This coupling induces hybridization of energy levels at the interface, generating chiral electronic states, which enables preferential emission of left or right CPL and endows the perovskite

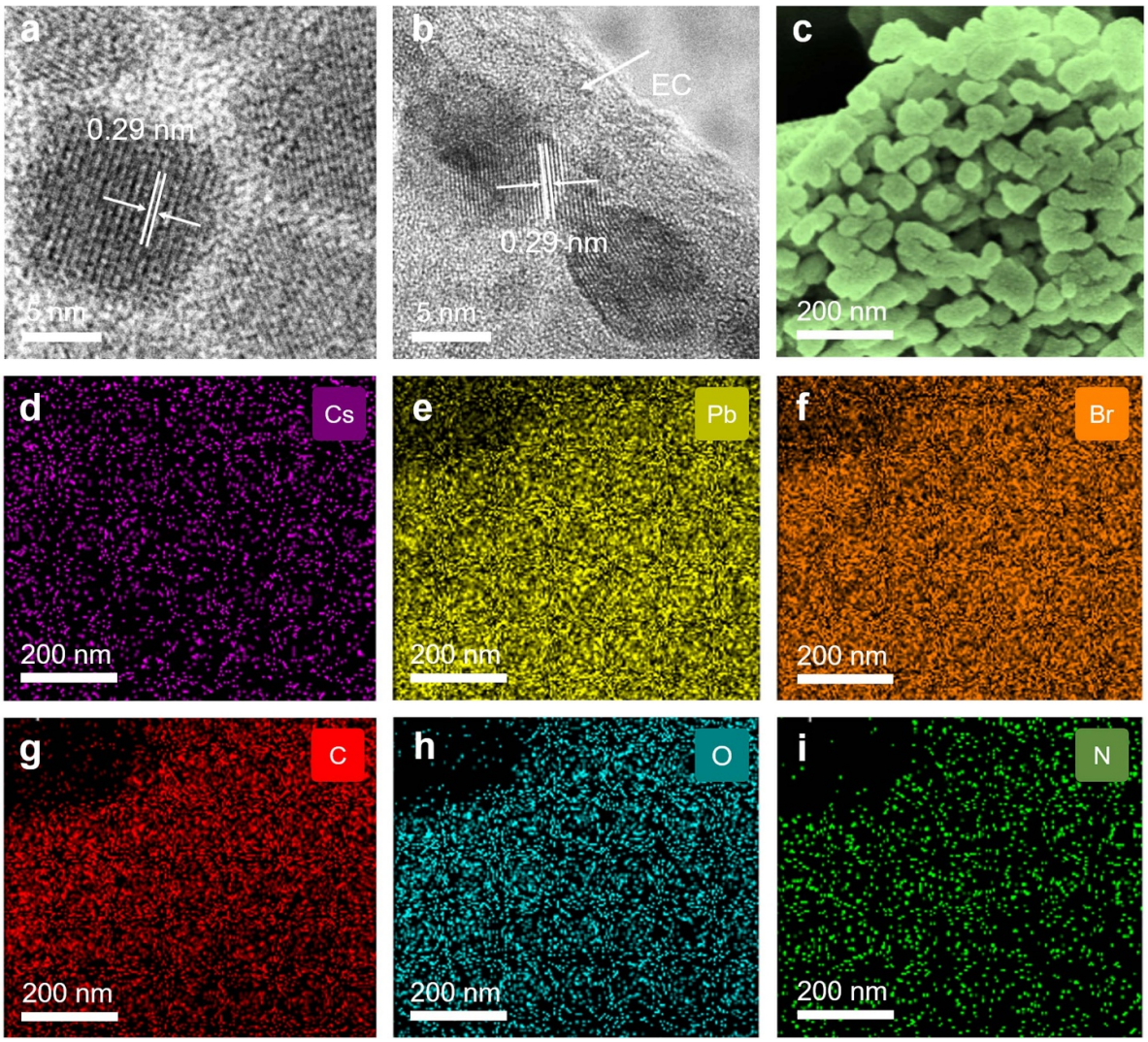

Figure 2. Microstructure and morphology of perovskite NCs/EC. HRTEM images of (a) $CsPbBr_3$, (b) $CsPbBr_3$/EC. (c) SEM image of the selected $CsPbBr_3$/EC and corresponding EDS mapping of (d) Cs, (e) Pb, (f) Br, (g) C, (h) O, and (i) N of selection area.

ink with chiral polarization light response properties [19, 38]. This phenomenon is also observed in this work, the CPL spectra (figure S5) reveal that unmodified $CsPbBr_3$/EC sample exhibits no detectable CPL signal, whereas the R-/S-DPEM modified $CsPbBr_3$/EC ink demonstrates clear left- and right-handed CPL emission characteristics. Furthermore, the CPL intensity and dissymmetry factor (g_{lum}) exhibit progressive enhancement with increasing concentrations of the chiral ligand, as observed in figures 4(a)–(c) and S6(a)–(c). Notably, the maximum g_{lum} values reached 2.7×10^{-3} for R-$CsPbBr_3$/EC and -3.4×10^{-3} for S-$CsPbBr_3$/EC at $n = 0.6$. It is worth noting that the introduction of EC effectively enhanced the CPL intensity of chiral perovskites (figure S7). The cross-linked network of EC forms a physical barrier around the NCs, significantly inhibiting the desorption of the surface chiral ligands under the influence of external factors. The obtained g_{lum} is comparative to reported relevant work (table S1). The strong interaction between chiral ligands and the surface of perovskite provides a strong foundation for the transfer of chirality [39], which is evidenced by shifts in the stretching vibration of N–H (from 3257 cm^{-1} to 3216 cm^{-1}) and bending vibration (from 1582 cm^{-1} to 1566 cm^{-1}) in FTIR, along with a downward shift in the Br 3d binding energy observed in XPS spectra (figures S8(a) and (b)). These findings highlight the substantial potential of chiral surface modification in enabling perovskite NCs to exhibit CPL activity.

In addition, red and blue chiral perovskite NCs inks were prepared by anion exchange on the base of $CsPbBr_3$/EC, their fluorescence digital photos and corresponding PL spectra are presented in figure 4(d). It can be seen that the inks display bright fluorescent emission and the PL spectra show narrow and pure light emission. The CPL is also observed in the blue and red emission, as shown in figures 4(e)–(g). Figures S9(a) and (b) show the corresponding g_{lum} value curves of

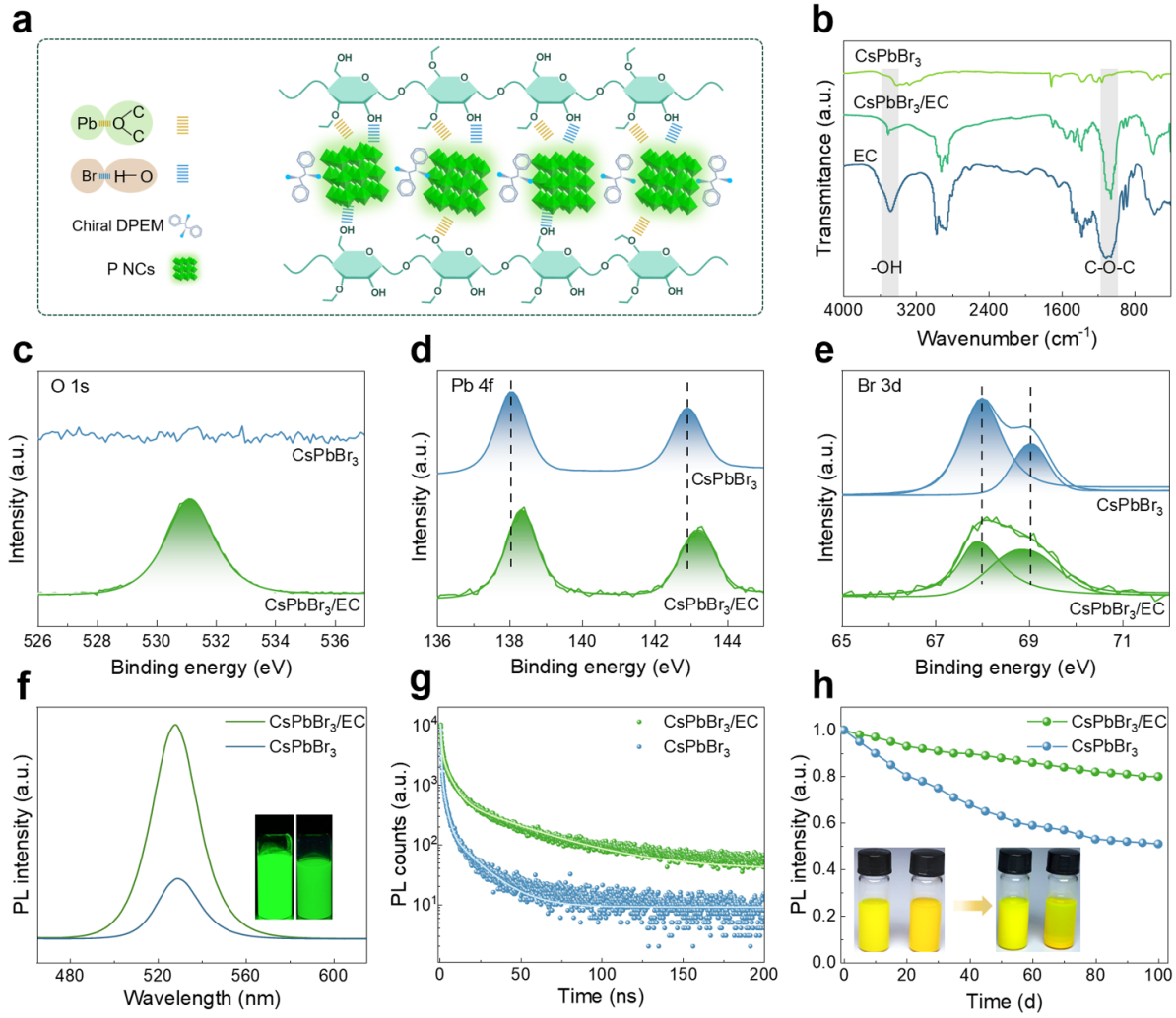

Figure 3. Chemical interaction and photoelectric properties of perovskite NCs/EC. (a) Mechanisms of interaction between perovskite NCs, EC, and chiral molecules. (b) FTIR spectra of EC, $CsPbBr_3$ and $CsPbBr_3$/EC. XPS spectra for (c) O 1s, (d) Pb 4f, (e) Br 3d. (f) PL spectra. (insets are photographs of $CsPbBr_3$/EC (left) and $CsPbBr_3$ (right) ink under UV light). (g) PL decay curves and (h) PL intensity attenuation under atmospheric environment (insets are photographs of $CsPbBr_3$/EC (left) and $CsPbBr_3$ (right) ink under natural light) of $CsPbBr_3$ and $CsPbBr_3$/EC ink.

$CsPb(Br/I)_3$ and $CsPb(Br/Cl)_3$, which reach the order of 10^{-4}. The successful preparation of chiral $CsPb(Br/I)_3$, $CsPbBr_3$ and $CsPb(Br/Cl)_3$/EC fluorescent inks demonstrates the universality of our strategy. More importantly, it paves the way for the fabrication of multicolor CPL inks and the design of multicolor CPL patterns.

Benefiting from the natural polymer material-EC, this system demonstrates dual functionalities: on the one hand, EC serves as a carrier that can load and protect chiral perovskite NCs; on the other hand, it imparts excellent processability to chiral perovskite NCs inks, thereby significantly expanding their potential application scenarios in the future. The fluidity and adhesion properties of the ink enable the customization of patterns through screen printing. Moreover, the presence of active group (hydroxyl) on the surface of EC ensures good compatible with various substrates. Figure 5(a) display photographs of leaf-shaped patterns printed on PTFE, Paper, PET and Fabric substrates under natural light and UV light. Among these, the sample on the paper surface exhibit the best uniformity, which can be attributed to the strong compatibility between the cellulose-based paper and the ink formulation. This highly malleable can also be compatible with a variety of patterning processing techniques. Figure 5(b) illustrates complex QR code patterns can be clearly fabricated and it can be successfully recognized by mobile phones. The uniform and bright 'SONG' and 'ZZU' words can also be printed on paper (figure S10(a)). Additionally, the chiral ink can also be directly handwritten, evidenced by characters 'CPL' in figure 5(c). Immersing nylon ropes into the ink allows for the fabrication of luminescent filaments (figure 5(d)). Furthermore, laser direct writing enables precise engraving of films into different shapes and patterns, for example,

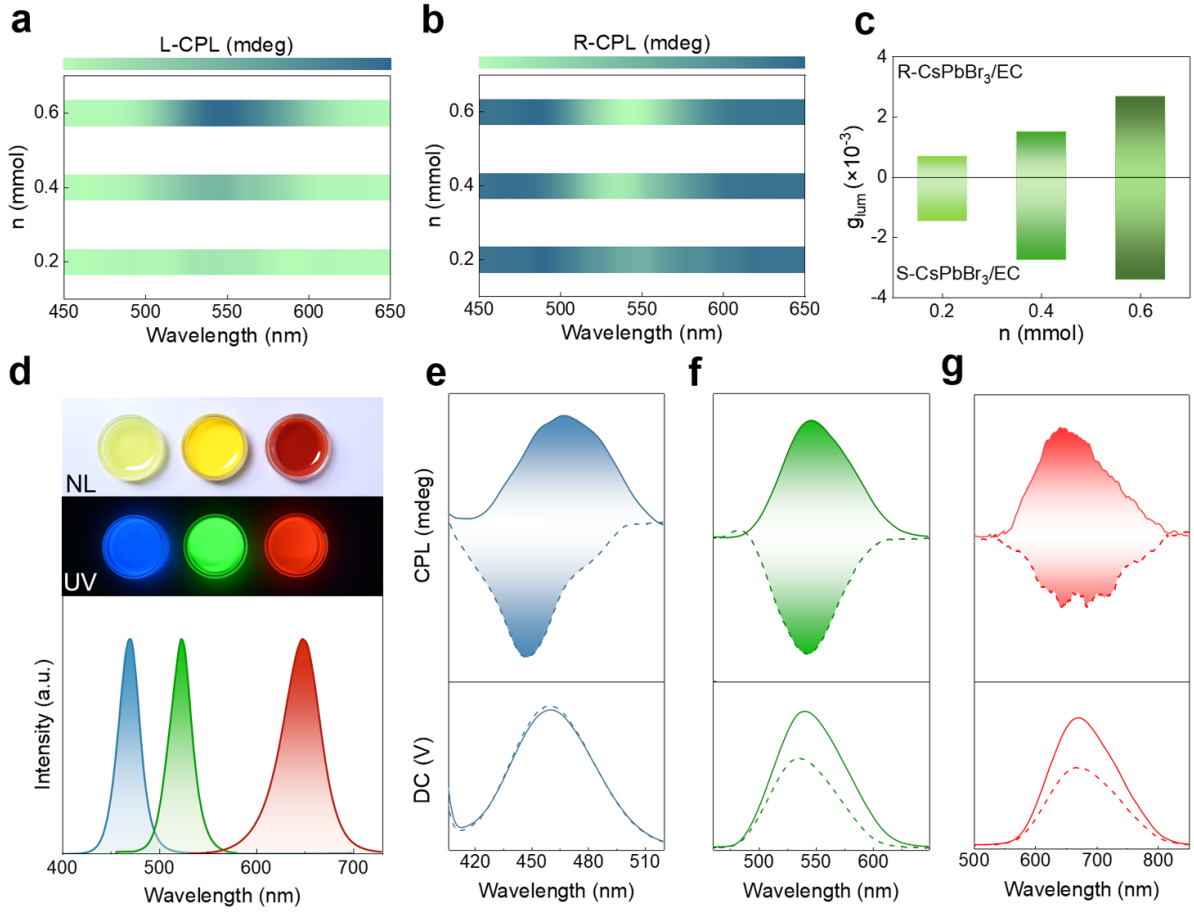

Figure 4. Circularly polarized luminescence performance of perovskite NCs/EC. The concentration-dependent CPL intensity of (a) R–$CsPbBr_3$/EC, (b) S–$CsPbBr_3$/EC and corresponding (c) g_{lum} values. (d) Photographs of typical blue ($CsPb(Br/Cl)_3$), green ($CsPbBr_3$) and red ($CsPb(Br/I)_3$) emitting chiral perovskite NCs/EC ink under natural and UV light and their corresponding PL spectra. CPL spectra and corresponding DC spectra of (e) blue, (f) green and (g) red emitting ink.

heart-shaped pattern (figure 5(e)), and intricate characters like 'Fu' (figure S10(b)). The diverse processing techniques and stable luminescent performance make chiral perovskite show promising application prospects in the field of preparing CPL patterns.

Notably, large-area CPL films can be fabricated using a coating machine. The films exhibiting blue, green and red emission are shown in figure 6(a), and the paper-like films have a certain information-carrying capacity for data encryption, as demonstrated by the laser-etched 'cellulose' characters. And the CPL signal of $CsPbBr_3$/EC film is also detected as shown in figure 6(b), which is consistent with the chiral ink, (R- and S-$CsPbBr_3$/EC films exhibit positive and negative CPL signals, respectively). The g_{lum} of the R-film is 2.6×10^{-3}, and that of the S-film is -3.1×10^{-3} (figure S11). In addition, we also tested the CPL at six different points across the S-$CsPbBr_3$/EC film and found that their g_{lum} almost remained consistent, demonstrating the uniformity of large-area $CsPbBr_3$/EC film (figure 6(c)). Furthermore, this cellulose film also exhibits uniform fluorescence, which is superior to that of perovskite film (figure S12).

Particularly, the film demonstrates outstanding flexibility and stability. As shown in figure 6(d), after twisting 1000 times, no cracks or holes are observed in the microscopic photograph, exhibiting the excellent flexibility of the $CsPbBr_3$/EC film. And the PL intensity also has hardly declined after twisting 1000 times (figure 6(e)). In addition, the luminescent film demonstrates excellent stability. After being stored in air at 50% humidity and room temperature for 70 d, the luminescence of pure perovskite film has almost completely lost, while the $CsPbBr_3$/EC film still maintains 80% of its initial intensity (figure S13). Under UV light, cellulose films can maintain 51% of their initial strength for 30 d, while $CsPbBr_3$ stops glowing after 10 d (figure S14). Furthermore, the EC-protected film demonstrates notable water resistance. After being immersed in water for 30 d, it retains approximately 60% of its original luminescence intensity, while pure perovskite films completely degrade within just 3 d of water

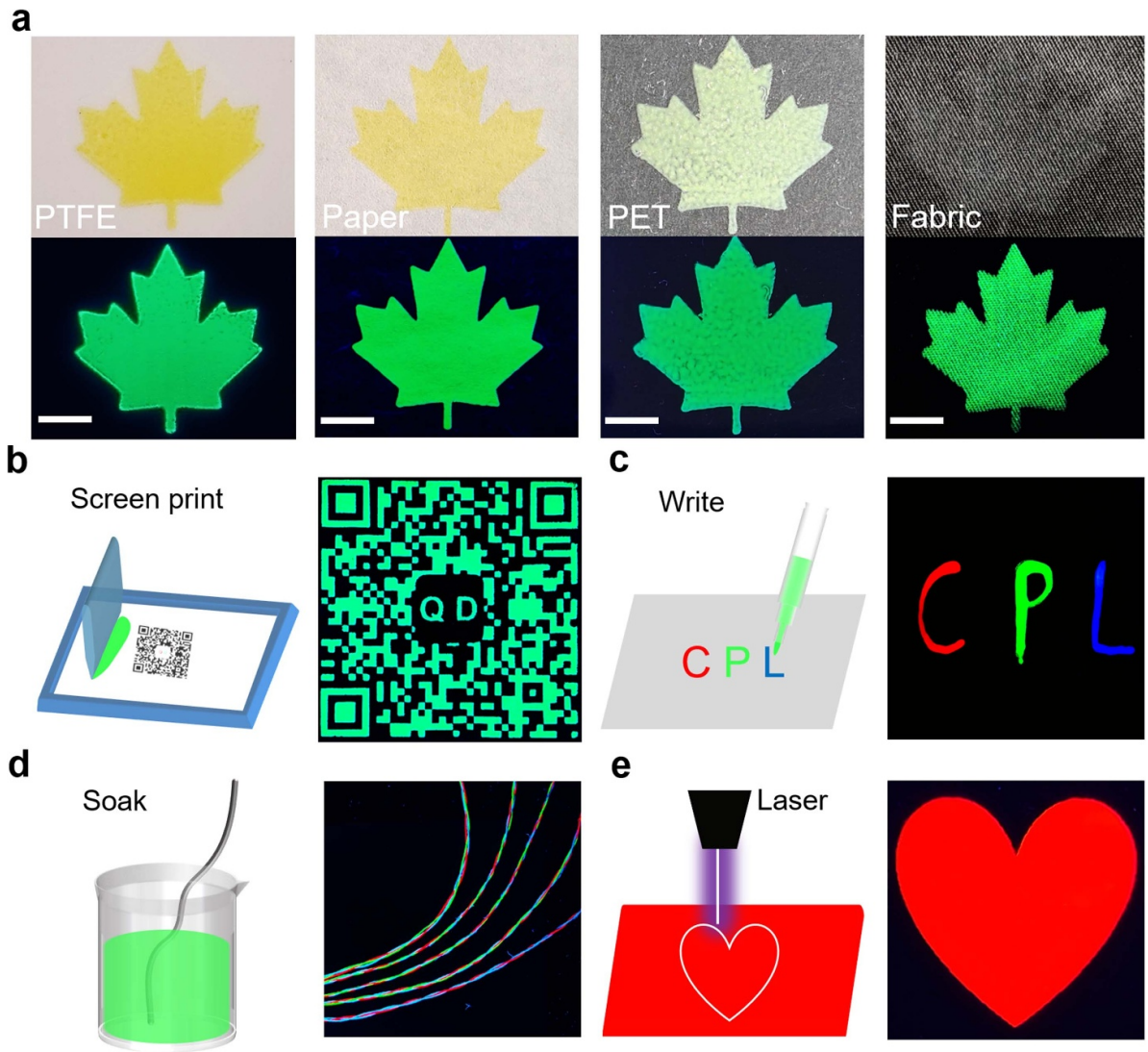

Figure 5. The processing technology of perovskite NCs/EC ink. (a) Photos of leaf-shaped patterns on PTFE, Paper, PET, and Fabric, the scale bar is 1 cm. Schematic diagrams of patterned (b) QR code via screen printing process, (c) 'CPL' draft via handwriting, (d) colorful fibers via soaking and (e) heart-shaped pattern via laser engraving.

immersion (figures 6(f) and S15). Notably, the composite film can be reprocessed, so it can be recycled when it is damaged (figure S16). Finally, R-/S-$CsPbBr_3$/EC film can be used as an efficient and stable CPL source for UV pumped CP-LEDs. A combination of a quarter-wave plate (QWP) and a linear polarizer (LP) can be used to detect CPL. QWP transforms the L- and R-handed CPL components into linearly polarized light oriented at $+45°$ and $-45°$ to its fast axis, respectively. The result is filtered with a LP and detected by the spectrometer. As shown in figure S17, the intensity of LCP measured by R-$CsPbBr_3$/EC is stronger than that of RCP, and the S-$CsPbBr_3$/EC is opposite, both of them are consistent with the test results of CPL spectrometer.

4. Conclusions

In summary, we successfully achieved large scale *in-situ* synthesis of chiral $CsPbBr_3$/EC inks at room temperature through a wet ball-milling method. The introduction of chiral ligands allows for tunable CPL intensity, achieving a maximum g_{lum} of -3.4×10^{-3} (S-$CsPbBr_3$/EC) when $n = 0.6$ mmol. Meanwhile, $CsPb(Br/I)_3$ and $CsPb(Br/Cl)_3$ inks with red and blue emission were prepared by anion exchange. The introduction of EC enables the chiral luminescent ink with excellent processability and compatible with multiple substrates, not only improving the environmental stability and luminescent properties of chiral perovskites, but also enabling precise patterning via screen printing and direct writing. Subsequently, large-area thin films were readily fabricated, and solid-state chiral luminescence was achieved. Thin-film patterning was also accomplished through laser engraving. More importantly, the $CsPbBr_3$/EC films exhibit excellent flexibility and environmental stability. In conclusion, our study demonstrates the feasibility of scalable preparation of chiral perovskite inks and provides a promising strategy for advancing the practical application of chiral perovskite materials.

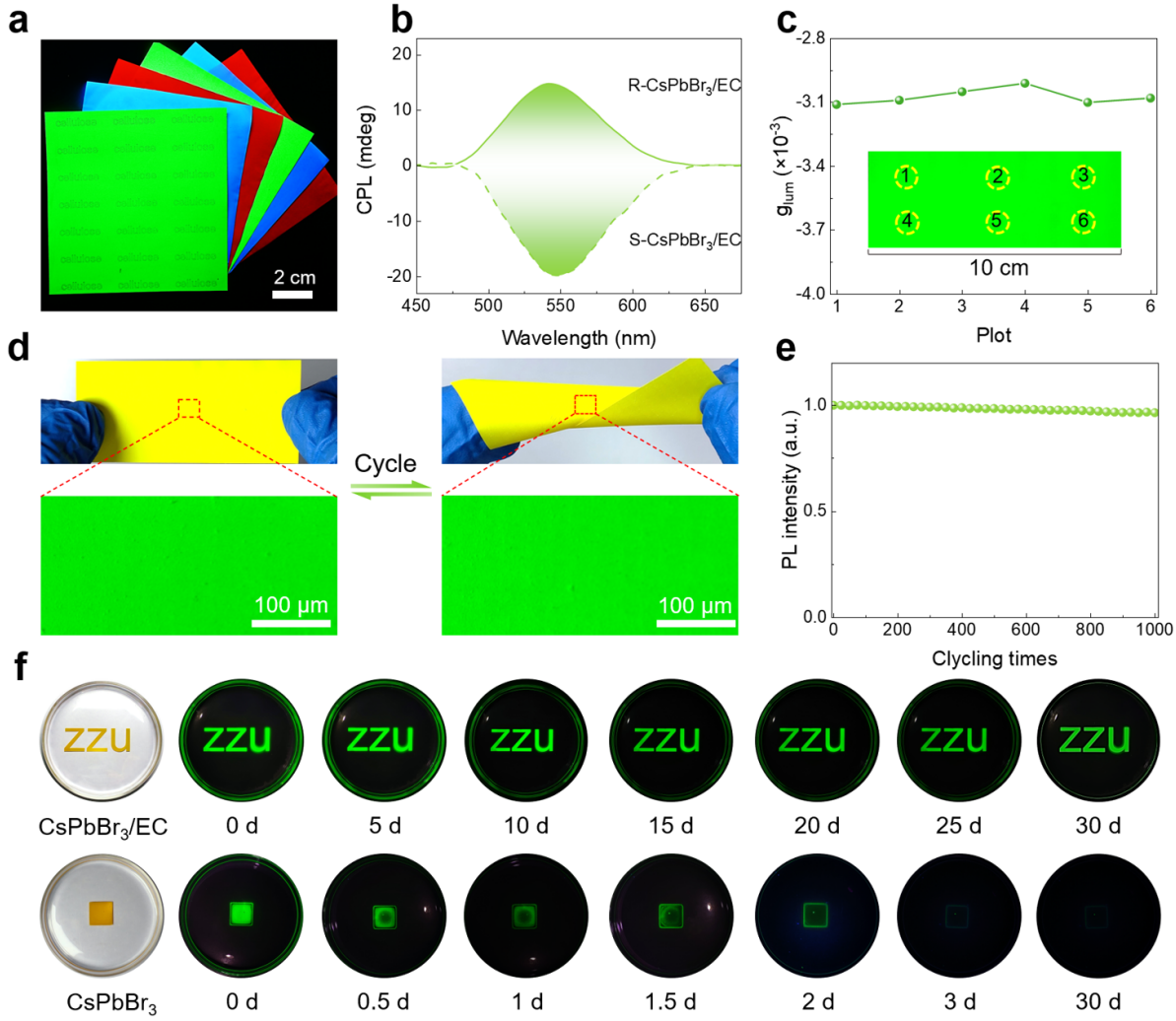

Figure 6. Flexibility and stability of perovskite NCs/EC films. (a) Photographs of large-area red, green, blue films under UV light, patterned words are engraved by laser. (b) Typical CPL spectra of $CsPbBr_3$/EC films with $n = 0.6$. (c) The g_{lum} values at the six points across the S–$CsPbBr_3$/EC film. (d) Photographs of film before and after 1000 twisting and their microscopic morphologies. (e) The variation of PL intensity under 1000 twisting. (f) The luminescent photographs of $CsPbBr_3$ and $CsPbBr_3$/EC patterned films soaking in water for 30 d.

5. Future perspectives

This study has successfully laid a solid foundation for the scalable synthesis and practical application of chiral perovskite materials. The introduction of EC has enhanced the stability and flexibility of chiral perovskites, making them potentially applicable to wearable devices. Future research should consider developing new chiral ligands and conducting in-depth analysis of the chiral transfer mechanism. Investigate the effects of chiral perovskites under various conditions such as nonlinear optics, magnetic fields, and electric fields. Develop new strategies to increase the g_{lum} of perovskite to meet practical application. At the same time, it is necessary to further enhance the stability of the materials, develop other scalable production processes, and promote the industrialization process. This is conducive to promoting the development of chiral perovskite materials towards a diverse technological revolution and interdisciplinary applications.

Acknowledgment

This work is supported by National Natural Science Foundation of China (Grant Nos. 52572185, 12204427 and 52272166), Natural Science Foundation of Henan Province of China (Grant Nos. 242300421217, and 222300420299).

Conflict of interest

The authors declare no competing financial interests.

Author's contributions

Boya Li: Writing—original draft, Methodology, Investigation, Formal analysis, Data curation, Conceptualization. Leimeng Xu: Writing—review & editing, Supervision, Methodology, Conceptualization, Funding acquisition.

Wenxuan Fan: Methodology, Formal analysis. Fangru Wang: Methodology, Formal analysis. Wanjie Wang: Methodology, Conceptualization. Jizhong Song: Writing—review & editing, Supervision, Methodology, Funding acquisition.

ORCID iDs

Leimeng Xu 0000-0002-2614-3742
Wanjie Wang 0000-0002-1508-891X
Jizhong Song 0000-0002-1606-4776

References

[1] Zhang M *et al* 2023 Processable circularly polarized luminescence material enables flexible stereoscopic 3D imaging *Sci. Adv.* **9** eadi9944
[2] Guo Q, Li Z, Zhou Y, Zhao S, Wang Y, Zhang M, Li G, Tong Z, Zhuang T and Yu S-H 2025 Self-positioning microdevices enable adaptable spatial displaying *Sci. Adv.* **11** eadv2721
[3] Huang Y *et al* 2024 Intense left-handed circularly polarized luminescence in chiral nematic hydroxypropyl cellulose composite films *Adv. Mater.* **36** 2308742
[4] MacKenzie L E and Pal R 2021 Circularly polarized lanthanide luminescence for advanced security inks *Nat. Rev. Chem.* **5** 109
[5] Tang J *et al* 2024 Chiral ionic liquids enable high-performance room temperature single junction spin-light emitting diodes *Laser Photon. Rev.* **19** 2401008
[6] Yao J, Wang Z, Huang Y, Xue J, Zhang D, Chen J, Chen X, Dong S-C and Lu H 2024 Efficient green spin light-emitting diodes enabled by ultrafast energy- and spin-funneling in chiral perovskites *J. Am. Chem. Soc.* **146** 14157
[7] Kitzmann W R, Freudenthal J, Reponen A P M, VanOrman Z A and Feldmann S 2023 Fundamentals, advances, and artifacts in circularly polarized luminescence (CPL) spectroscopy *Adv. Mater.* **35** 2302279
[8] Zhang K, Fan W, Yao T, Wang S, Yang Z, Yao J, Xu L and Song J 2024 Polymer-surface-mediated mechanochemical reaction for rapid and scalable manufacture of perovskite QD phosphors *Adv. Mater.* **36** 2310521
[9] Song J, Li J, Li X, Xu L, Dong Y and Zeng H 2015 Quantum dot light-emitting diodes based on inorganic perovskite cesium lead halides ($CsPbX_3$) *Adv. Mater.* **27** 7162
[10] Xu L, Li J, Cai B, Song J, Zhang F, Fang T and Zeng H 2020 A bilateral interfacial passivation strategy promoting efficiency and stability of perovskite quantum dot light-emitting diodes *Nat. Commun.* **11** 3902
[11] Fan W, Wang S, Yang Z, Yao J, Xu L and Song J 2025 In situ formation of luminescent perovskite quantum dot/polymer composites: scalable synthesis, continuous processing and functional applications *Adv. Mater.* **37** 2505600
[12] Ma S, Ahn J and Moon J 2021 Chiral perovskites for next-generation photonics: from chirality transfer to chiroptical activity *Adv. Mater.* **33** 2005760
[13] Ding Z, Chen Q, Jiang Y and Yuan M 2024 Structure-guided approaches for enhanced spin-splitting in chiral perovskite *JACS Au* **4** 1263
[14] Liang B, Zhang L, Jiang Y, Chen S and Yuan M 2023 Metal halide perovskites: promising materials toward next-generation circularly polarized luminescence *J. Mater. Chem. C* **11** 4993
[15] Yang C H *et al* 2023 In situ formed perovskite nanocrystal films toward efficient circularly polarized electroluminescence *Adv. Funct. Mater.* **34** 2310500
[16] Chen D, Tang B, Sergeev A A, Wu Y, Liu H, Zhu D, Hu S, Wong K S, Yip H-L and Rogach A L 2025 Green spin light-emitting diodes enabled by perovskite nanocrystals in situ modified with chiral ligands *ACS Energy Lett.* **10** 815
[17] Kim Y-H *et al* 2020 Strategies to achieve high circularly polarized luminescence from colloidal organic–inorganic hybrid perovskite nanocrystals *ACS Nano* **14** 8816
[18] Mendoza-Carreño J, Molet P, Otero-Martínez C, Alonso M I, Polavarapu L and Mihi A 2023 Nanoimprinted 2D-chiral perovskite nanocrystal metasurfaces for circularly polarized photoluminescence *Adv. Mater.* **35** 2210477
[19] Jiang S, Song Y, Kang H, Li B, Yang K, Xing G, Yu Y, Li S, Zhao P and Zhang T 2021 Ligand exchange strategy to achieve chiral perovskite nanocrystals with a high photoluminescence quantum yield and regulation of the chiroptical property *ACS Appl. Mater. Interfaces* **14** 3385
[20] Tao L, Zhan H, Cheng Y, Qin C and Wang L 2023 Enhanced circularly polarized photoluminescence of chiral perovskite films by surface passivation with chiral amines *J. Phys. Chem. Lett.* **14** 2317
[21] Ye C, Jiang J, Zou S, Mi W and Xiao Y 2022 Core–shell three-dimensional perovskite nanocrystals with chiral-induced spin selectivity for room-temperature spin light-emitting diodes *J. Am. Chem. Soc.* **144** 9707
[22] Ma J, Fang C, Chen C, Jin L, Wang J, Wang S, Tang J and Li D 2019 Chiral 2D perovskites with a high degree of circularly polarized photoluminescence *ACS Nano* **13** 3659
[23] Lin J T, Chen D G, Yang L S, Lin T C, Liu Y H, Chao Y C, Chou P T and Chiu C W 2021 Tuning the circular dichroism and circular polarized luminescence intensities of chiral 2D hybrid organic–inorganic perovskites through halogenation of the organic ions *Angew. Chem., Int. Ed.* **60** 21434
[24] Zhang X, Li L, Chen Y, Valenzuela C, Liu Y, Yang Y, Feng Y, Wang L and Feng W 2024 Mechanically tunable circularly polarized luminescence of liquid crystal-templated chiral perovskite quantum dots *Angew. Chem., Int. Ed.* **63** e20240420
[25] Fiuza-Maneiro N, Mendoza-Carreño J, Gómez-Graña S, Alonso M I, Polavarapu L and Mihi A 2024 Inducing efficient and multiwavelength circularly polarized emission from perovskite nanocrystals using chiral metasurfaces *Adv. Mater.* **36** 2413967
[26] Yang X, Zhou M, Wang Y and Duan P 2020 Electric-field-regulated energy transfer in chiral liquid crystals for enhancing upconverted circularly polarized luminescence through steering the photonic bandgap *Adv. Mater.* **32** 2000820
[27] Cao Y, Liu Y, Shang X, Lin Y, Lin L, Zhang N, Gao H and Chen X 2025 Full-color circularly polarized luminescence from perovskite quantum dots embedded within chiral zif-8 matrix *Nano Today* **62** 102730
[28] Liu J-Z, Chai X-Y, Huang J, Li R S, Li C M, Ling J, Cao Q-E and Huang C Z 2024 Chiral assembly of perovskite nanocrystals: sensitive discrimination of amino acid enantiomers *Anal. Chem.* **96** 4282
[29] Kim M, Kim J, Bang J, Jang Y J, Park J and Kim D H 2023 Simultaneously achieving room-temperature circularly polarized luminescence and high stability in chiral perovskite nanocrystals via block copolymer micellar nanoreactors *J. Mater. Chem. A* **11** 12876
[30] Wen Z, Lu R, Gu F, Zheng K, Zhang L, Jin H, Chen Y, Wang S and Pan S 2022 Enabling efficient blue-emissive circularly polarized luminescence by in situ crafting of chiral quasi-2D perovskite nanosheets within polymer nanofibers *Adv. Funct. Mater.* **33** 2212095
[31] Wang Y, Cheng Y, Yin C, Zhang J, You J, Wang J, Wang J and Zhang J 2024 Manipulating crystal growth and secondary phase PbI_2 to enable efficient and stable perovskite solar cells with natural additives *Nano-Micro Lett.* **16** 183

[32] Song Y H, Choi S H, Yoo J S, Kang B K, Ji E K, Jung H S and Yoon D H 2017 Design of long-term stable red-emitting $CsPb(Br_{0.4}, I_{0.6})_3$ perovskite quantum dot film for generation of warm white light *Chem. Eng. J.* **313** 461
[33] Jin B, Ren L, Gou Y, Ma R, Liang Z, Li Z, Dong B, Zhao L, Wang S and Wu C 2023 Fiber-bridging-induced toughening of perovskite for resistance to crack propagation *Matter* **6** 1622
[34] Yang J *et al* 2019 Extremely low-cost and green cellulose passivating perovskites for stable and high-performance solar cells *ACS Appl. Mater. Interfaces* **11** 13491
[35] Kwon B, Park J, Choi W, Song H and Oh J H 2025 Ligand-driven chirality in perovskites for advanced optoelectronics *ACS Appl. Mater. Interfaces* **17** 54356–79
[36] Kim Y-H *et al* 2022 The structural origin of chiroptical properties in perovskite nanocrystals with chiral organic ligands *Adv. Funct. Mater.* **32** 2200454
[37] Jin X, Zhou M, Han J, Li B, Zhang T, Jiang S and Duan P 2021 A new strategy to achieve enhanced upconverted circularly polarized luminescence in chiral perovskite nanocrystals *Nano Res.* **15** 1047
[38] Long G, Sabatini R, Saidaminov M I, Lakhwani G, Rasmita A, Liu X, Sargent E H and Gao W 2020 Chiral-perovskite optoelectronics *Nat. Rev. Mater.* **5** 423
[39] Son J *et al* 2023 Unraveling chirality transfer mechanism by structural isomer-derived hydrogen bonding interaction in 2D chiral perovskite *Nat. Commun.* **14** 3124